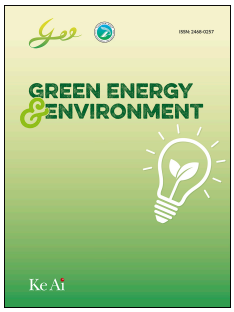

Novel Magnetic Carbon Supported Molybdenum Disulfide Catalyst and Its Application in Residue Upgrading

Xiangyang Zhu, Dong Qiao, Liangrong Yang, Qinling Bi, Huifang Xing, Shan Ni, Menglei Yuan, Huizhou Liu, Luhai Wang, An Ma

PII: S2468-0257(20)30098-4

DOI: https://doi.org/10.1016/j.gee.2020.06.025

Reference: GEE 259

To appear in: *Green Energy and Environment*

Received Date: 10 April 2020

Revised Date: 1 June 2020

Accepted Date: 24 June 2020

Please cite this article as: X. Zhu, D. Qiao, L. Yang, Q. Bi, H. Xing, S. Ni, M. Yuan, H. Liu, L. Wang, A. Ma, Novel Magnetic Carbon Supported Molybdenum Disulfide Catalyst and Its Application in Residue Upgrading, *Green Energy & Environment*, https://doi.org/10.1016/j.gee.2020.06.025.

Graphical abstract:

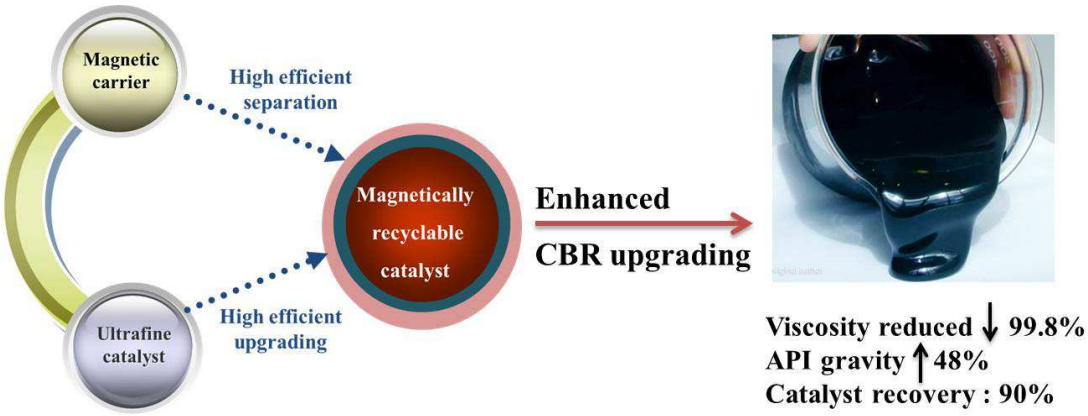

In this work, for the first time, we report the magnetically retrievable Fe_3O_4/C-MoS_2 catalysts by a synergistic strategy that achieves enhanced hydrocracking performance for the actual heavy oil upgrading.

Novel Magnetic Carbon Supported Molybdenum Disulfide Catalyst and Its Application in Residue Upgrading

Xiangyang Zhu, [ab] Dong Qiao, [c] Liangrong Yang, [*ab] Qinling Bi, [d] Huifang Xing, [ab] Shan Ni, [ab] Menglei Yuan, [ab] Huizhou Liu, [*a b] Luhai Wang[d] and An Ma[d]

[a]CAS Key Laboratory of Green Process and Engineering, State Key Laboratory of Biochemical Engineering, Institute of Process Engineering, Chinese Academy of Sciences, Beijing 100190, China. E-mail: lryang@ipe.ac.cn; hzliu@ipe.ac.cn

[b]School of Chemical Engineering, University of Chinese Academy of Sciences, Beijing 100049, China

[c]China University of Petroleum, Beijing 102249, China

[d]Petrochemical Research Institute, Petrochina, Beijing, 102206, China

ABSTRACT

A novel hybrid material consisted of carbon covered Fe_3O_4 nanoparticles and MoS_2 nanoflower (FCM) was designed and prepared by micelle-assisted hydrothermal methods. Multiple techniques, including X-Ray diffraction (XRD), high-resolution transmission electron microscopy (HRTEM) and X-ray photoelectron spectroscopy (XPS) were employed to characterize it. The results show that FCM has a flower-like morphology with a 330 nm Fe_3O_4 core as well as 70 nm highly crystalline MoS_2 shell. FCM is superparamagnetic with a saturation magnetization of 35 emu/g. Then

hydrocracking of Canadian bitumen residue (CBR) was applied to estimate its catalytic activity. The results show that FCM exhibits superior catalytic hydrocracking activity compared to bulk MoS_2 and commercial oil-dispersed $Mo(CO)_6$ by the same Mo loading. Further measurement by elemental analysis, XPS and XRD reveals that the MoS_2 nanoflower with abundant catalytic active sites and covered carbon layer with anti-coke ability donate to the superior upgrading performance. Besides, the catalysts can be easily recovered by the external magnetic field. This work provides a novel kind magnetic nanocatalyst which is potential for slurry-phase hydrocracking applications.

Keywords: Magnetic; Carbon; MoS_2; Catalyst; Heavy oil

1. Introduction

Catalytic hydrocracking is an essential component in refinery and petrochemical industries and is also one of the most important means to convert various heavy and inferior feeds into high-quality fuel, lube base oil and chemical raw material [1–7]. The effective catalysts such as finely-powdered (e.g. ores with a high content of iron, molybdenum and nickel) and soluble catalysts (e.g. water-soluble salts and oil-soluble salts of molybdenum, iron or vanadium) have been extensively investigated [8,9]. Among them, MoS_2 has attracted continuous attraction as one of the main active catalysts because of its strong hydrogenation power, superior coke suppression and desulfurization activities [10–12]. Catalyst separation and recovery have become a bottleneck for its applications, catalysts present in the oil products also affect the

quality and stability of the oil products [13–16]. Besides, the catalytic activity of these catalysts needs to be further improved, Lee et al. reported that MoS_2 formed by oil-soluble precursor such as $Mo(CO)_6$ (in-situ sulfidation) have drawbacks such as poor dispersibility and loss of active sites due to the growth of its size and stacking number in the reaction conditions [17].

Magnetite (Fe_3O_4), with a cubic inverse spinel structure, has emerged as ideal catalysts or supports due to its low cost, easy preparation, size controllable and paramagnetic nature [18–21]. Introducing magnetic particles as cores can facilitate the fast and efficient hydrocracking catalysts recycling and avoid affecting product quality and stability [22–24]. On the other hand, molybdenum disulfide nanosheets can be dispersed and wrapped outside the nanoscale magnetic cores, enhancing the catalyst activity by increasing the number of active sites and further stabilizing the catalyst [24]. Zheng et al have prepared $MoS_2/SiO_2/Fe_3O_4$ catalysts and then tested for hydrodesulfurization of dibenzothiophene as a model compound [25]. However, the SiO_2 coating layer couldn't efficiently protect the Fe_3O_4 core from sulfidation in the high sulfur environment of the realistic heavy oil conditions, which was mentioned in their later report [26]. Carbon materials have attracted wide attention benefiting from their good acid and base resistance, low cost and high thermal stability, anti-coke ability [27–31]. It may have a better protective effect than SiO_2. Du et al. revealed the synergistic effect of MoS_2 and carbon by density functional theory and x-ray photoelectron spectroscopy, which exhibited outstanding catalytic activity for residue hydrocracking [32]. Moreover, compared with hydrophilic SiO_2, carbon has lipophilic

properties that are more prone to disperse in heavy oil.

Herein, we report the novel synthesis of catalysts that consist of 330 nm Fe_3O_4 as the core, which coated with carbon as the protective layer and then loaded with flower-like MoS_2. Furthermore, the newly designed catalyst was applied for hydrocracking of residue and the catalytic activity was compared to commercial oil-soluble $Mo(CO)_6$ and bulk MoS_2. Among all, FCM showed a comparable result: 99.80% of viscosity reduction rate, 37% of hydrodenickelation and 20% of hydrodevanadium rate during the 30 min tests, the catalyst can be easily recovered from the product under an external magnetic field. This study provides new insights into the design and synthesis of novel highly efficient recyclable catalysts for heavy oil upgrading.

2. Experimental Section

2.1 Materials

Ferric chloride hexahydrate ($FeCl_3 \cdot 6H_2O$>99%) was of analytical grade and purchased from Xilong Chemical Industry Co. Ltd. (Shantou, China). Polyvinylpyrrolidone (PVP K-30, Mw= 40,000) and ammonium acetate (NH_4Ac) were obtained from Sigma–Aldrich Corp. Ltd. (St Louis, MO, USA). Ammonium acetate, Ammonium molybdate tetrahydrate ($(NH)_6Mo_7O_{24} \cdot 4H_2O$) and thiourea ($CH_4N_2S$>99%) were purchased from Sinopharm Chemical Reagent Co. Ltd. (Beijing, China). All these reagents were used without any further purification. Molybdenum hexacarbonyl ($Mo(Co)_6$, Sigma-Aldrich, 98%) were used as reference samples.

2.2 Catalysts preparation

Monodisperse Fe_3O_4 nano-spheres were synthesized through a one-pot solvothermal process with the presence of NH_4Ac as the structure-directing agent as described previously [33]. Typically, 30 mmol $FeCl_3 \cdot 6H_2O$ was dissolved in 300 mL of ethylene glycol, followed by the addition of 0.25 mol NH_4Ac under magnetic stirring. The resulting mixture was transferred to a 500 mL Teflon-lined autoclave and then maintained at 200 °C for 12 h. After the reaction, the autoclave was cooled to room temperature. The black colloidal particles were then washed 5 times with deionized water and separated by magnetic decantation.

Fe_3O_4/C-MoS_2 was prepared by a one-pot polyvinylpyrrolidone (PVP) micelle-assisted hydrothermal method. Firstly, a certain amount of PVP (K-30, Mw= 40 000) was dissolved in 300 mL of distilled water with stirring at room temperature for 1 h. Next, 3.08 g of ammonium molybdate tetrahydrate $(NH_4)_6Mo_7O_{24} \cdot 4H_2O$ and 7.21 g of thiourea (CH_4N_2S) were added into the PVP solution. After stirred for 1 h, 2.0 g Fe_3O_4 nano-spheres prepared previously were added to the mixture solution and stirred for another hour. The mixture was transferred into a 500 mL Teflon-lined stainless steel autoclave and heated at 200 °C for 24 h and then the precipitates were separated from the solution by a hand-held magnet (neodymium). Afterward, the particles were washed five times with deionized water and then dried at 60 °C. At last, the intermediates were annealed at 800 °C for 2 h under Ar atmosphere to carbonize PVP and

improve the crystallinity of MoS_2. MoS_2 nanoflower was prepared by a similar procedure without the addition of Fe_3O_4.

2.3 Catalyst characterization

The FT-IR analysis was carried out by a Bruker T27 FT-IR spectrophotometer between 4000 and 500 cm^{-1} using the KBr pellet technique, with a resolution of 2 cm^{-1}. The morphology of catalysts was determined by scanning electron microscopy (SEM, JEOL JSM-6700F, Japan). As-synthesized Fe_3O_4 spheres were dispersed in ethanol and sonicated to ensure a uniform dispersion. The magnetic property of Fe_3O_4 spheres and FCM was measured by vibrating sample magnetometry (VSM; Model 4 HF VSM, ADE Technologies, USA). X-ray diffraction (XRD, X'PERT PRO MPD diffractometer, Cu Kα radiation, λ = 0.15418 nm, scanned a range of 5–90°) was used to identify the crystal structure of all prepared catalysts. Transmission electron microscopy (TEM, JEM-2100F) was utilized to investigate the morphology of all samples. X-ray photoelectron spectroscopy (XPS) data were collected using a PHI Quantera II monochromatized Al Ka cathode source of 75–150 W under ultrahigh vacuum. Inductively coupled plasma optical emission spectrometry (ICP-OES) was utilized to quantify the molar contents of Fe, Ni, V, etc.

2.4 Catalyst performance tests and characterization

The reactor system used for this experiment is shown in **Figure S1**. The feed oil used for the hydroconversion experiments was CBR and the properties

of CBR are listed in **Table S1**. A 500 mL stirred autoclave reactor (0-1200 rpm) was used to assess different catalysts in a batch mode at a reaction temperature of 415℃, initial H_2 pressure of 10 MPa, and a reaction time of 30 min. For this study, 200 g of feedstock was taken into the reactor and 0.10 g as prepared catalyst (500 ppm) was mixed with the hydrocarbon feed. The reactor was sealed and checked for leakage by nitrogen. Next, H_2 was purged to remove all gas impurities. At the beginning of the reaction, the mixture was stirred at 300 rpm and the temperature was increased from room temperature to 200℃ at a rate of 5℃/min. Then increased H_2 pressure to 10 MPa, the rotating speed was further increased to 800 rpm for about 1 h. Afterward, the reactor was heated to 415℃ in 40 min; the autoclave was heated at 415℃ for 30 min under constant stirring. After each reaction test, the autoclave was cooled down to room temperature and the gaseous product was vented. Liquid products were collected manually using a syringe and the catalysts were recovered using $Nd_2Fe_{14}B$ magnet. The size of the magnet used is 40 mm*20 mm*5 mm and its maximum tensile strength is 820 g. Then manually separate the catalysts from the magnet. The recovered solids were washed with diesel oil to remove diesel oil-soluble materials, followed by drying in a vacuum oven at 120 °C for 3−4 h until the weight became constant. For comparison, the reactions without catalysts were performed under the same condition. For comparison, MoS_2 and commercial $Mo(CO)_6$ were also used under the same reaction condition.

For the liquid products, the C, H, N and S contents were determined by elemental analysis (Vario MACRO cube), while Ni, V, Fe, Ca and the other elements contents were analyzed by inductived coupled plasma atomic emission spectroscopy (ICP-AES). The component analyses of four groups (saturate, aromatic, resin and asphaltenes) in the heavy oil were conducted according to the test method of NB/SH/T 0509-2010. Asphaltenes were precipitated from crude oil by n-heptane, saturates, aromatics and resins were rinsed by n-heptane, methylbenzene and methylbenzene and alcohol, respectively. Then, the viscosity and API gravity of CBR was recorded by the programmable viscometer (Brookfield DV-III). The viscosity reduction rate (VRR) of CBR was calculated by the method as below:

$$VRR = \frac{u_1 - u_2}{u_1} \quad (1)$$

u_1: heavy oil viscosity before upgrading without additives; u_2: heavy oil viscosity after upgrading with additives.

3. Results and discussion

3.1 Catalyst Characterization

As displayed in **Figure 1**, scanning electron microscopy (SEM) and transmission electron microscopy (TEM) results show the morphologies of different catalysts. It can be found that the fabricated Fe_3O_4 particles have an average diameter of about 330 nm (**Figure 1a**). The Fe_3O_4 nanoparticles are used as a catalyst carrier because of their fast, efficient and recycling abilities [34]. MoS_2 nanoflowers have a diameter ranging from 170 to 200 nm (**Figure 1b, 1e** and **1f**), the surfaces of these

microspheres manifest distinct nanoflakes-like morphology, signifying the existence of hierarchical structure [35]. FCM was prepared by one-pot polyvinylpyrrolidone (PVP) micelle-assisted growth of MoS_2 on the surface of Fe_3O_4 nanoparticles using $(NH_4)_6Mo_7O_{24}$ and excess thiourea as precursors. The results show that FCM has a flower-like morphology with 330 nm Fe_3O_4 core as well as 70 nm highly crystalline MoS_2 shell. (**Figure 1c**). HR-TEM was applied to further confirm the microstructure of FCM, as shown in **Figure 1g, 1h** and **1i.** The lattice d-spacing is calculated to be 0.64 nm, which corresponds to the (002) plane of MoS_2. The fast Fourier transform (FFT) of the image in the inset of **Figure 1i** shows the lattice symmetry well matched with the (002) and (100) planes of MoS_2 [36]. The high-angle dark field scanning transmission electron microscopy (HAADF-STEM) (**Figure S2**) and the corresponding energy-dispersive X-ray spectroscopy (EDS) element mapping results further reveal the nanoparticles and nanoflowers shapes which correspond to Fe_3O_4 and C-MoS_2, respectively. **Figure S3** shows the infrared spectra of the synthesized Fe_3O_4 NPs (a) and FCM (b). The peak at 557 cm^{-1} can be ascribed to the stretching band of the Fe-O bonds [37], proving the existence of Fe_3O_4. Besides, a weak vibrational peak at 476 cm^{-1} is attributed to the stretching mode of the Mo-S linkage of MoS_2 nanosheets [38]. All of these results are in agreement with the results of the SEM and TEM observations.

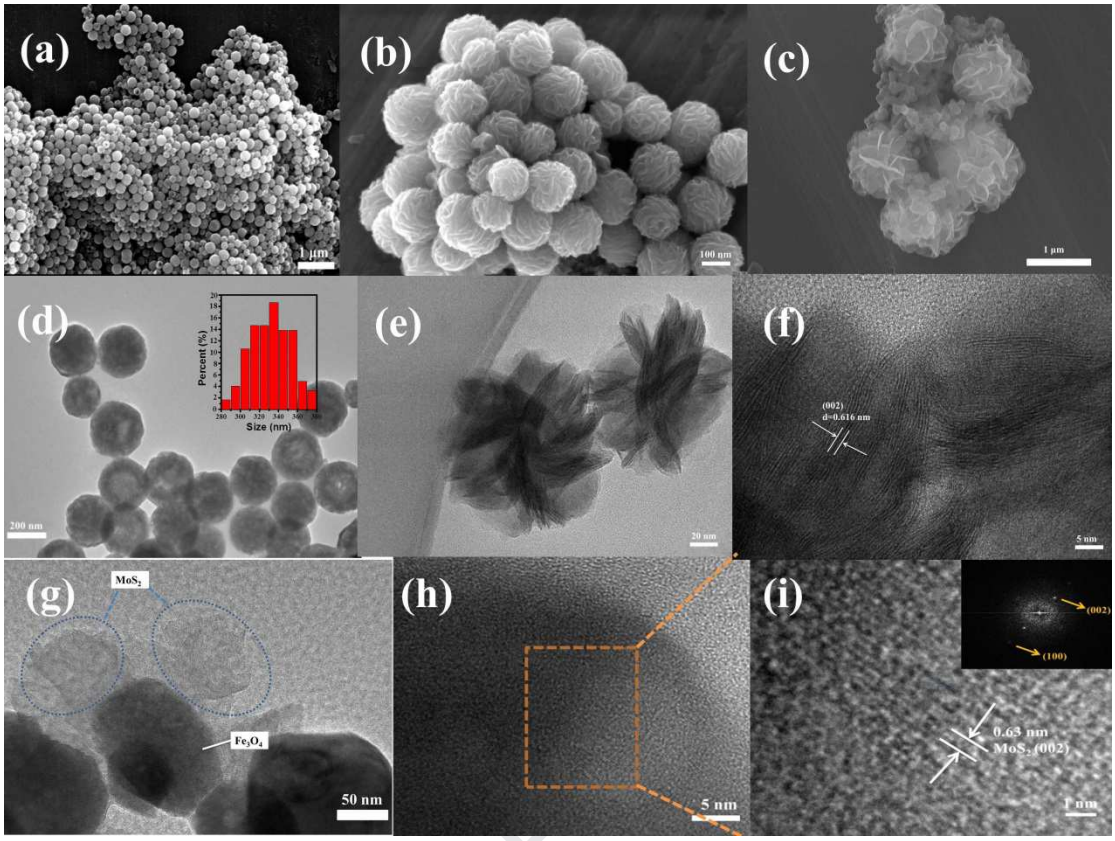

Figure 1. SEM images of (a) Fe_3O_4, (b) MoS_2 and (c) FCM; TEM images of (d) Fe_3O_4 (inset is the corresponding size distributions) and (e) MoS_2; (f) HR-TEM images of MoS_2; (g) TEM images of FCM; (h) Few layered MoS_2 in FCM; (i) HR-TEM images of MoS_2 in FCM (inset is the corresponding FFT image).

The surface chemical composition and valence states of the samples were further confirmed by X-ray photoelectron spectroscopy analysis (XPS). The survey spectrum of FCM manifests the existence of S, Mo, C, O and Fe elements (**Figure 2a**). In the high-resolution of Fe 2p spectrum (**Figure 2b**), two peaks at 725.3 eV and 711.1 eV can be assigned to Fe $2p_{1/2}$ and Fe $2p_{3/2}$, and the binding energy at 713.3 eV represents Fe^{3+} oxide states, suggesting there exist Fe_3O_4 in FCM [39–41]. On the other hand, the high-resolution S 2p spectrum (**Figure 2c**) shows the existence of S $2p_{1/2}$ and S $2p_{3/2}$ of S^{2-} at 163.7 eV and 168.8 eV, the binding energy at 170.2 eV corresponds to S_2^{2-}, indicating the partial oxidation of S^{2-} [39,42]. **Figure 2d** depicts the Mo $3d_{3/2}$ and Mo $3d_{5/2}$

dominant peaks of Mo in MoS_2 at 232.6 eV and 229.5 eV, a weak peak corresponds to the Mo^{6+} is obtained at 235.5 eV, which should be derived from MoO_4^{2-} or MoO_3, suggesting the partial oxidation of the catalyst in the air [43]. Moreover, the O 1s spectrum shown in **Figure S4** can be convoluted into three spectral bands at 532.6, 531.5 and 530.0 eV, corresponding to the physically adsorbed H_2O, the surface hydroxyl groups and the crystal lattice oxygen, respectively [44,45].

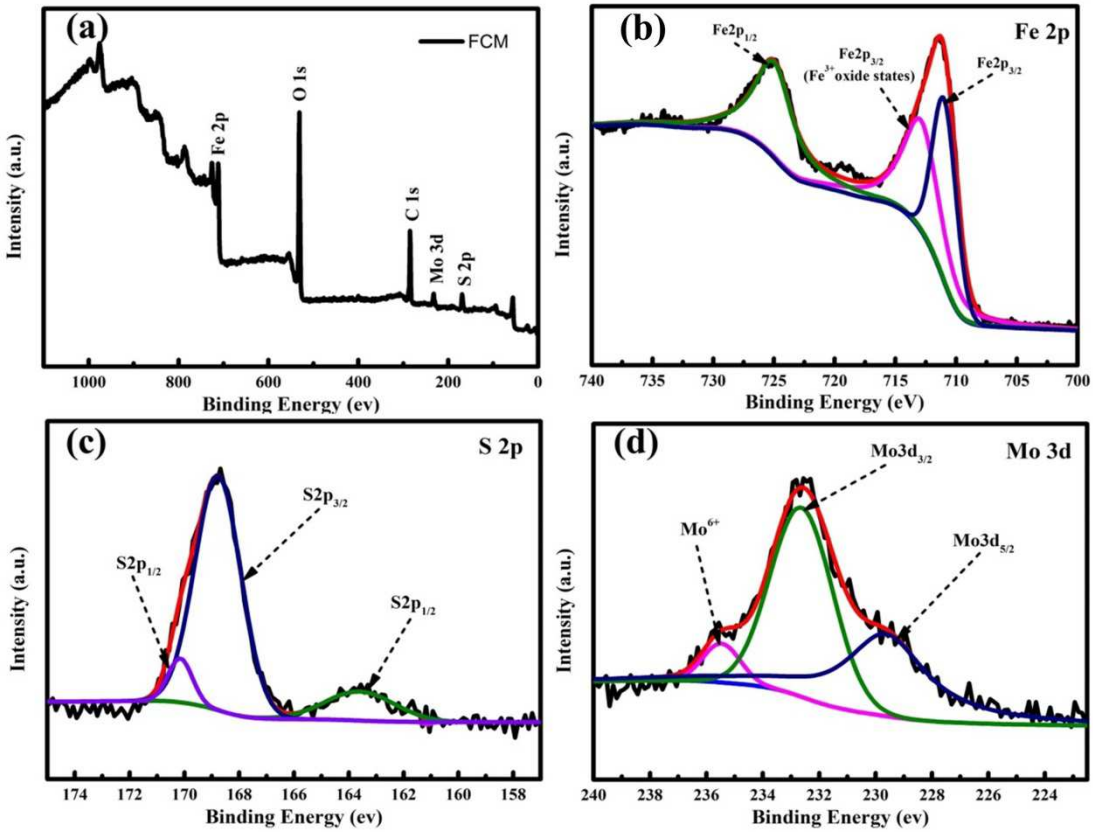

Figure 2. (a) XPS survey spectra of FCM. (b, c and d) High-resolution XPS spectrum of Fe 2p (b), S 2p (c) and Mo 3d (d).

The crystalline structure of the as-prepared Fe_3O_4 and FCM were characterized by XRD (**Figure 3a**). All the diffraction peaks of Fe_3O_4 match well with the standard card (JCPDS 89–2355) [46] and the strong diffraction peaks at 30.08°, 35.43°, 43.06° and 62.53° correspond to the (220), (311), (400)

and (440) planes of face-centered cubic Fe_3O_4, suggesting its high crystallinity. Compared with Fe_3O_4, new diffraction peaks at 14.40°, 32.69° and 39.57° matching the amorphous MoS_2 phase (JCPDF 87–2416), no other peaks have been observed. The results indicated that Fe_3O_4/C-MoS_2 composites are formed at the reaction conditions [47]. **Figure S5** shows the XRD pattern of the MoS_2, the diffraction peaks at 14.38°, 29.03°, 32.68°, 33.51°, 35.87°, 39.54°, 49.79° and 58.33° are observed, which are assigned to (002), (004), (100), (101), (102), (103), (105) and (110) planes of the hexagonal MoS_2 (JCPDS No.37-1492) [48]. As for the $Mo(CO)_6$ sample (**Figure S6**), the peak at 15.5°, 20.1°, 28.5°, 35.1°, 42,4°, 56.7°, 66.2°, 73.3° can respectively be indexed to the (101), (201), (102), (222), (103), (004), (044), (015) planes of hexacarbonyl molybdenum (JCPDS: 75-1336).

A magnetization test was performed to investigate the effect of MoS_2 on the magnetic properties of FCM, as shown in **Figure 3b**, saturation value for bare magnetite particles and FCM are 82 emu g^{-1} and 34.87 emu g^{-1} respectively. With such high saturated magnetization, FCM catalysts could be quickly separated from the products with the aid of an external magnetic field.

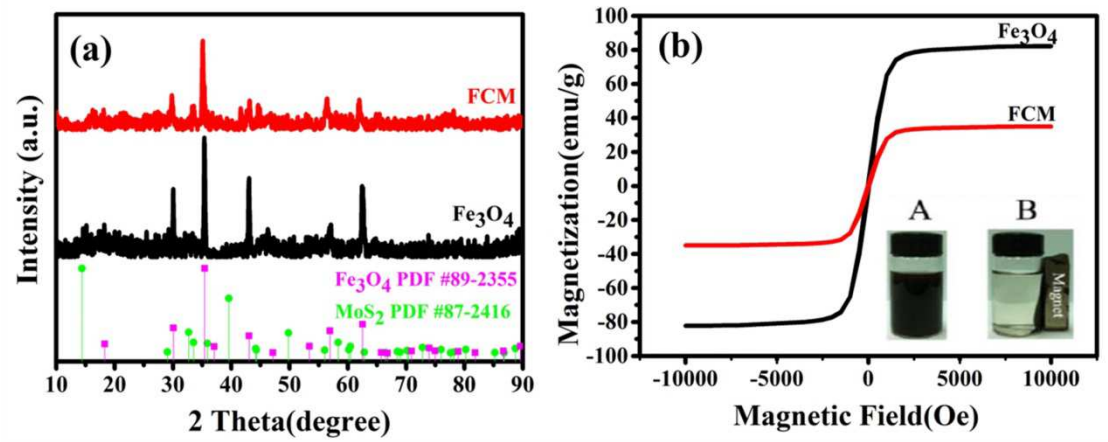

Figure 3. (a) Experimental XRD patterns of as-prepared catalysis; (b) Magnetization curves for Fe_3O_4 and FCM measured at 298K. (The inset illustrates the magnetic separation of FCM from aqueous solution under the application of an external magnetic field and the time from (A) to (B) was less than 30 seconds.)

3.2 Catalytic performance

The hydrocracking effects of catalysts were evaluated using the reactor assembling given in **Figure S1**. The process includes a three-phase reaction including fine catalyst, H_2, and high molecular weight oil CBR. The type of catalyst is thus an important factor affecting the reaction.[49,50] To test the H_2 taking capacity of the different catalysts in the CBR hydrocracking process, hydrocracking without catalyst is regarded as a reference standard. **Figure S7a** presented the temperature and pressure files of the hydrocracking process. **Figure S7b** shows the reactor pressure profile for the effects of different catalysts. In normal operation, the initial condition was set 10.0 MPa at 200 °C, and the reactor pressure increased to about 13.0 MPa upon the temperature ramping to 415 °C. In the presence of the catalyst, the pressure of the reactor decrease due to H_2 consumption prevailing via hydrocracking.[49] All catalysts except $Mo(Co)_6$ exhibit the same trend of pressure decrease. Because $Mo(CO)_6$ is an oil-soluble catalyst, it has better dispensability in oil and more

opportunities to contact with hydrogen. Therefore, the hydrogen pressure is rapidly reduced due to catalytic hydrocracking when the reactor temperature reaches nearly 380℃. The same trend was also reported by Yong-Kul Lee [51]. As displayed in **Figure S7b**, when the reaction progressed to about 10 minutes, the H_2 pressure began to drop due to H_2 consumption prevailing via hydrocracking. However, in the reaction stage, the H_2 pressure curve without catalyst hardly changes, thus we can conclude that the fabricated FCM catalyst has the hydrocracking ability.

The test was performed with the same load of catalysts (500 ppm) and in the catalyst hydrocracking processes, MoS_2 is the main active component [52]. Through the ICP measurement, the Mo content for MoS_2, $Mo(CO)_6$ and FCM was calculated to be 599.3 mg/g, 363.4 mg/g and 204.1 mg/g respectively. Because Fe_3O_4 and MoS_2 are the main components of FCM, we also prepared Fe_3O_4 and MoS_2 for comparison (**Table S2)**. Of note, the fabricated MoS_2 catalyst showed a similar viscosity reduction activity with the commercial MoS_2. However, the fabricated Fe_3O_4 catalyst showed poor viscosity reduction activity. **Figure 4** shows the viscosity reduction per unit Mo of CBR after hydrocracking with FCM, MoS_2 and $Mo(CO)_6$. The viscosity of CBR before catalytic hydrocracking is 56600 cP. It can be seen that MoS_2, FCM and $Mo(CO)_6$ can effectively reduce the viscosity of CBR. After hydrocracking without catalyst, the viscosity decreased to 83.8 cP. But a large amount of thermal coke can be seen attached to the agitator at the end of this process (**Figure S8**). The high production of thermal coke reduced the upgraded crude oil yield, these problems make the non-catalyzed hydrocracking reaction commercially unavailable [9].

However, no thermal coke was found when tested in the presence of different catalysts. Surprisingly, we find that FCM has a better performance than oil-soluble $Mo(CO)_6$ and MoS_2. The viscosity reduction per unit active component follows the order: FCM > $Mo(CO)_6$ > MoS_2. According to the "Rim-Edge" model [53], the amorphous MoS_2 leads to more unsaturated S atoms at the edges, thereby increasing the active sites available for reaction. Furthermore, the weak metal–support interaction effect in the C-MoS_2 catalyst resulted in the negligible formation of coke and inhibited the growth of MoS_2 during the reaction [54]. The results indicate that the generated MoS_2 nanoflower with abundant active sites and covered carbon layer with anti-coke ability donate to the superior upgrading performance. While bulk MoS_2 or $Mo(CO)_6$ can easily aggregate to form longer crystals with more layer, resulting in loss of active sites of the catalyst [55].

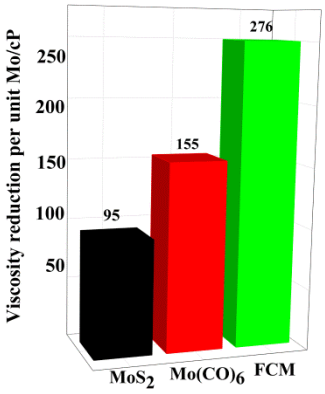

Figure 4. The variation of viscosity reduction per unit Mo with different catalysts.

The infrared spectrums of CBR before and after upgrading with different catalysts are displayed in **Figure 5a**. It is used to analyze the changes of functional groups from the view of molecules. The peaks at the 2860 cm^{-1} and 1376 cm^{-1} are assigned to symmetrical stretching vibration and symmetrical deformation vibration of methyl. While the peaks at 2925 and 1460 cm^{-1}

assigned to methylene in the CBR after the reaction was stronger, which suggested that the aromatics ring-opening reactions went on during the process [56]. Besides, the peaks at 1603 and 1705 cm^{-1} assigned to carbon-carbon double bond and carbonyl groups of aromatics hydrocarbons were weaker after reactions with different catalysts, which implied that the hydrogenations of the unsaturated groups during the process of the reaction [57,58].

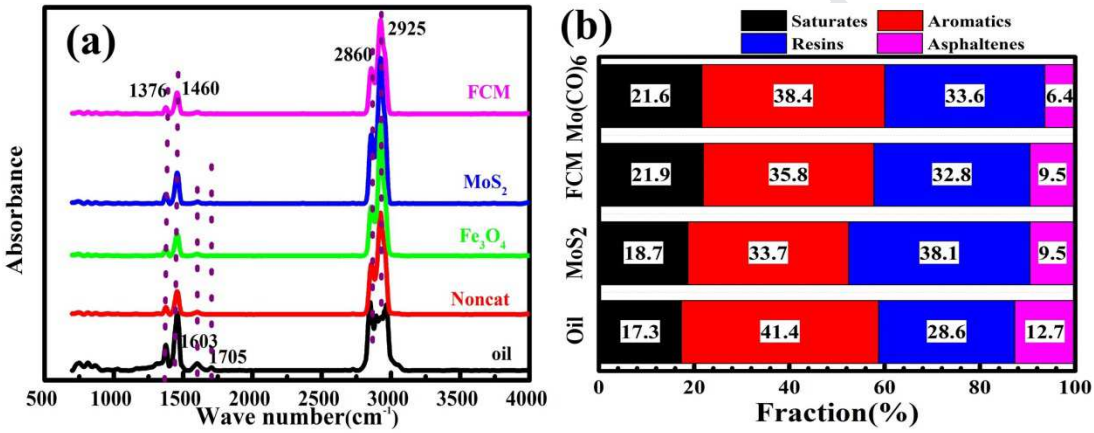

Figure 5. (a) The FT-IR spectrum of CBR before and after upgrading with different catalysts; (b) SARA analysis of CBR before and after hydrocracking with different catalysts.

The changes of SARA (saturates, aromatics, resins, and asphaltenes) composition of CBR before and after hydrocracking are summarized in **Figure 5b**. It could be seen that the portion of aromatics and asphaltenes decreased while the amount of light components saturates and resins in the CBR increased after the reactions, which could be attributed to the dissociation of asphaltenes macromolecules, thus leading to the viscosity reduction of CBR [59].

The elemental analysis of CBR before and after hydrocracking with different catalysts was illustrated in **Table S3.** The initial sulfur content in CBR was 5.144 wt%, after hydrocracking without catalyst, 4.505 wt%, in other

words, the removal conversion was 12.4%. The sulfur conversion rate for MoS_2, FCM and commercial $Mo(Co)_6$ catalysts was 16.01, 34.8 and 31.7% respectively. The HDS activity follow the order FCM > commercial $Mo(Co)_6$ > MoS_2.

Table 1 shows the metal analysis of oil samples before and after the reaction. When the test was performed by using FCM, about 90% of catalysts can be recovered from the oil products, however, when using MoS_2 or $Mo(CO)_6$, a large amount of metal molybdenum have been introduced artificially, which are harmful to the next step of oil treatment. Metal compounds such as V and Ni are harmful to catalytic processes [60], which may result in the corrosion of fluid catalytic cracking (FCC) catalysts [61] and the deactivation of hydrotreating catalysts. Therefore, the removal of metal compounds is important to heavy oil processing [62]. Based on the above metal analysis, it can be concluded that FCM has better metal (V and Ni) removal efficiency than MoS_2 or $Mo(CO)_6$, the concentration of vanadium and nickel was decreased by 63 mg/kg and 56 mg/kg, which is thought to be the decomposition of the CBR during the reaction [63].

Table 1 Metal analysis of CBR before and after upgrading with different catalysts.

Metal analysis	CBR	CBR+FCM	CBR+MoS_2	CBR+$Mo(CO)_6$
Ni (mg/Kg)	151	95	121	101
V (mg/Kg)	326	263	304	265
Fe (mg/Kg)	50	83	45	43
Mo (mg/Kg)	17.1	23	377	155

3.3 Activity of recycled catalyst

Catalyst recycling is critical to the slurry hydrocracking process; however, very few studies have reported the use of recycled (both supported and unsupported) catalysts in the process as stated in the introduction [13]. The stability of the FCM composite was investigated by reusing the catalyst for CBR upgrading. Traditional catalysts used in slurry-phase hydrocracking are usually separated by high-speed centrifugation, which is expensive and time-consuming. In contrast, the magnetic separation method has the advantages of convenience, simplicity, high efficiency, rapidity and suitable for mass production [64–66]. After the reaction, the magnet was put into the oil product and almost all the catalysts went straight towards the magnet within 3 minutes. When the magnet was removed from the oil product, it could be seen that a large number of solids adhered tightly to the surface of the magnet (**Figure S9**). Recycling of the catalyst is very essential for the slurry-phase hydrocracking process, the first recycle run of the test was repeated three times and the best recovery rate of the catalyst is about 90%. To investigate the activity of the recovered catalyst, another round of reaction was assessed at the same conditions. The viscosity of CBR after hydrocracking with the recovered catalyst was 121 cP at 50℃, only a slight decrease in catalytic activity (99.7% in viscosity reduction) compared to the freshly added catalyst (99.8% in viscosity reduction) and no thermal coking was seen after the reaction. It indicated that the catalyst still maintained its catalytic activity and coke suppression ability.

To investigate the changes in the crystal structure of the FCM, XRD analysis was performed (**Figure 6a**). MoS_2 has three characteristic peaks corresponding to the (003), (101) and (110) planes at 14.49°, 33.07° and 58.36°, no peak corresponding to the (002) plane of MoS_2 was observed in the diffraction pattern. The lack of a reflection corresponding to the (002) plane indicates the existence of highly dispersed crystallites with only a few atomic layers, which have higher hydrogenation activity than crystalline MoS_2 that shows a prominent (002) peaks [15]. Since a large amount of S was present in the feed, a sharp peak at 43.83° characteristic of pyrrhotite-4H ($Fe_{1-x}S$) was observed in the recovered catalyst. Attar and Martin postulated that the $Fe_{1-x}S$ facilitate the transfer of molecular hydrogen to organically bound hydrogen and plays a catalytic role in coal liquefaction[67]. Yang et al found that the (Fe, Ni)$_9S_8$ phases exist in catalysts, should be responsible for the high hydrogenation activity by using density functional theory calculations and experiment. The newly formed composites may also promote the hydrocracking of heavy oil[68].

Figure 6b shows the SEM images of the catalyst recovered from the oil sample after upgrading. The surface of carbonaceous material became a little bit smooth in the recovered catalyst. This suggested that a mild catalytic coke had formed on the catalyst surface. The magnetic properties of the recovered catalyst were also studied using VSM. As is shown in **Figure S10**, the saturation magnetization values for the recovered FCM were 8.9 emu/g.

Although the magnetism of the recovered catalyst decreased, it still has a good separation property under an external magnetic field.

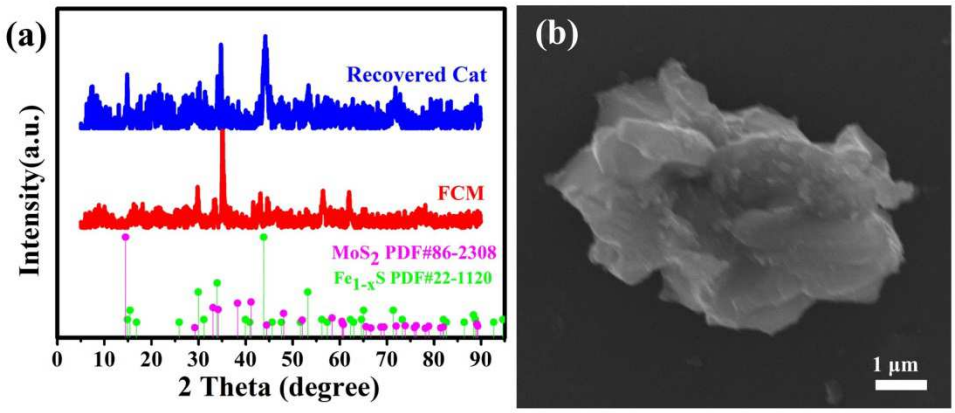

Figure 6. (a) XRD patterns of FCM and recovered catalyst; (b) SEM image of recovered catalyst;

To gain further insight into the possible changes of catalysts, the XPS survey spectra of FCM before and after the upgrading were collected (**Figure 7**). As shown in **Figure S11**, C, Fe, O, Mo and S were all present in the survey spectrum. The relative atomic concentrations of C, Fe, O, Mo, S, Ni and V listed in **Table S3** shown that the carbon content increased and the O, Fe content decreased. Furthermore, vanadium was detected at the surface of the recovered catalyst. It demonstrates that vanadium deposited on the surface of the catalyst may cause the decrease of catalyst activity. Because of the low concentration of vanadium in the catalyst after upgrading (compared to oxygen), further analysis of vanadium can't be done because of the overlapping between vanadium and oxygen [69]. As shown in **Figure 7a** of the oxygen spectra, the binding energy values increased slightly with 532.7 eV for O-H, 531.5 eV for Mo-O and 530.0 eV for Fe-O in comparison with the fresh sample, suggesting that the ratios between O-H, Mo-O and Fe-O were changed after upgrading

[43,70]. The ratio of O-H, Mo-O and Fe-O on the catalyst surface account for 15.9%, 55.7% and 28.4% before upgrading, respectively, whereas it accounted for 39%, 32.5% and 28.5% after upgrading, suggesting the fraction Mo-O decreased during the upgrading process, which might originate from the sulfided of molybdenum oxide in the high sulfur environment. The XPS characterization of the FCM catalyst above found that the catalyst was partially oxidized to MoO_3 in the air, but in the high temperature and high sulfur environment of heavy oil evaluation, MoO_3 was sulfided in situ into MoS_2, that's why the Mo-O decreased during after reaction. The catalytic activity of FCM was further enhanced with the increase of sulfurization degree. While the ratio of Fe-O remains unchanged, indicating that Fe_3O_4 can still exist stably under the reaction conditions. The carbon shell protects the Fe_3O_4 cores against damage from harsh chemical environments. While for the Fe 2p XPS spectra before and after upgrading, the Fe $2p_{3/2}$ binding energy values of the catalyst after upgrading decreased slightly to 710.8 (711.5 eV for the fresh catalyst), indicating the alternation of ratios of Fe(Ⅱ) and Fe(Ⅲ) after hydrocracking process [41]. Based on the deconvolution of Fe(Ⅱ) and Fe(Ⅲ) envelop, Fe(Ⅱ) and Fe(Ⅲ) accounted for 52.7% and 47.3% before upgrading, respectively, and for 13.4% and 86.6% afterward. The alternation indicates that the Fe^{2+} ions react with the CBR and Fe^{3+} was formed.

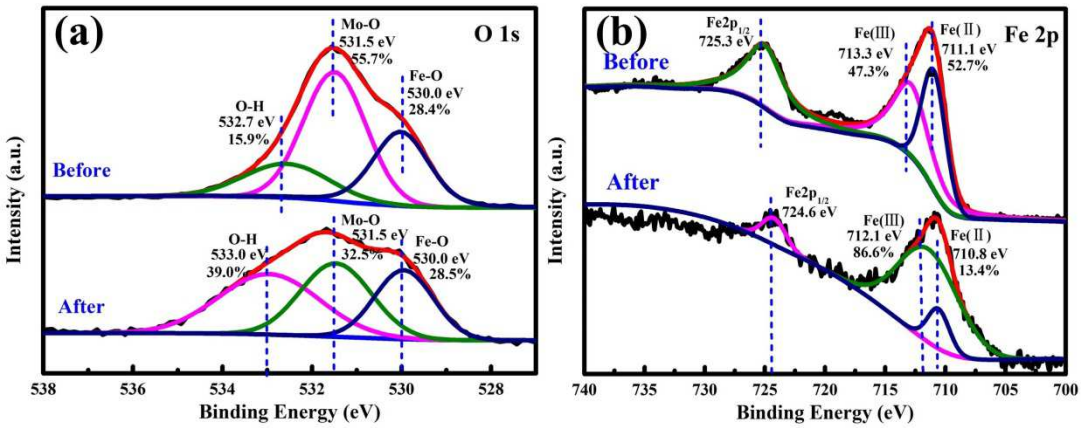

Figure 7. (a) O 1s XPS spectrum before and after upgrading. (b) Fe 2p XPS spectrum before and after upgrading.

4.0 Conclusions

In summary, the magnetically retrievable Fe_3O_4/C-MoS_2 catalysts used for heavy oil upgrading were successfully synthesized by a simple micelle-assisted hydrothermal strategy. Benefiting from the synergy effect between MoS_2 and carbon support, the prepared Fe_3O_4/C-MoS_2 catalysts exhibited superior hydrocracking performance, which reduced the viscosity of heavy oil by 99.8%, increased the API from 6.9 to 13.2 and hydrodenickelation and hydrodevanadium rate reached 37% and 20%, respectively. Furthermore, the catalyst can be easily recovered from the product without affecting its quality and stability. The designed catalyst has the advantage of high catalytic efficiency and ease for separation which is promising for industrial application.

Conflicts of interest

There are no conflicts to declare.

Acknowledgments

We would like to thank the following financial support: The National Natural Science Foundation of China (21922814, 21921005, 21676273,

21961160745, U1507203, 31961133019), the Youth Innovation Promotion Association, CAS (Grant Nos. 2016043), Beijing Natural Science Foundation (20194086) and China Petroleum Enterprise Cooperation Project (PRIKY17094).

References

[1] T. Parsell, S. Yohe, J. Degenstein, T. Jarrell, I. Klein, E. Gencer, B. Hewetson, M. Hurt, J.I. Kim, H. Choudhari, B. Saha, R. Meilan, N. Mosier, F. Ribeiro, W.N. Delgass, C. Chapple, H.I. Kenttämaa, R. Agrawal, M.M. Abu-Omar, Green Chem. 17 (2015) 1492–1499.

[2] F. Saleem, K. Zhang, A. Harvey, Chem. Eng. J. 356 (2019) 1062–1069.

[3] P. Šimáček, D. Kubička, G. Šebor, M. Pospíšil, Fuel 88 (2009) 456–460.

[4] J. Zecevic, G. Vanbutsele, K.P. De Jong, J.A. Martens, Nature 528 (2015) 245–254.

[5] C. Martínez, A. Corma, Coord. Chem. Rev. 255 (2011) 1558–1580.

[6] A. Tirado, J. Ancheyta, Renew. Energy 148 (2020) 790–797.

[7] V.L. Mangesh, S. Padmanabhan, P. Tamizhdurai, S. Narayanan, A. Ramesh, J. Hazard. Mater. 386 (2020) 121453.

[8] Y. Wang, Y. Chen, J. He, P. Li, C. Yang, Energy and Fuels 24 (2010) 1502–1510.

[9] A. Quitian, J. Ancheyta, Energy and Fuels 30 (2016) 10117–10125.

[10] T.A. Al-Attas, S.A. Ali, M.H. Zahir, Q. Xiong, S.A. Al-Bogami, Z.O. Malaibari, S.A. Razzak, M.M. Hossain, Energy and Fuels 33 (2019) 7917–

7949.

[11] M.S. Rana, V. Sámano, J. Ancheyta, J.A.I. Diaz, Fuel 86 (2007) 1216–1231.

[12] R. Sahu, B.J. Song, J.S. Im, Y.P. Jeon, C.W. Lee, J. Ind. Eng. Chem. 27 (2015) 12–24.

[13] A. Quitian, J. Ancheyta, Energy & Fuels 30 (2016) 4419–4437.

[14] M. Kouzu, Y. Kuriki, K. Uchida, K. Sakanishi, Y. Sugimoto, I. Saito, D. Fujii, K. Hirano, Energy and Fuels 19 (2005) 725–730.

[15] H. Rezaei, X. Liu, S.J. Ardakani, K.J. Smith, M. Bricker, Catal. Today 150 (2010) 244–254.

[16] K.H. Kang, G.T. Kim, S. Park, P.W. Seo, H. Seo, C.W. Lee, J. Ind. Eng. Chem. 76 (2019) 1–16.

[17] S.-H. Kim, K.-D. Kim, Y.-K. Lee, J. Catal. 347 (2017) 127–137.

[18] D. Wang, D. Astruc, Chem. Rev. 114 (2014) 6949–6985.

[19] V. Polshettiwar, R. Luque, A. Fihri, H. Zhu, M. Bouhrara, J.M. Basset, Chem. Rev. 111 (2011) 3036–3075. [20] T.D. Nguyen, Nanoscale 5 (2013) 9455–9482.

[21] X. Zhu, S. Ni, Q. Bi, L. Yang, H. Xing, H. Liu, Prog. Chem. 31 (2019) 381–393.

[22] I. Mochida, K. Sakanishi, R. Sakata, K. Honda, T. Umezawa, Energy and Fuels 8 (1994) 25–30.

[23] R. Liu, S. Dou, M. Yu, R. Wang, J. Clean. Prod. 168 (2017) 1048–1058.

[24] D. Lu, H. Fan, K.K. Kondamareddy, H. Yu, A. Wang, H. Hao, M. Li, J. Shen,

ACS Sustain. Chem. Eng. 6 (2018) 9903–9911.

[25] S. Sharifvaghefi, Y. Zheng, ChemCatChem 7 (2015) 3397–3403.

[26] S. Sharifvaghefi, Y. Zheng, ChemistrySelect 2 (2017) 4678–4685.

[27] S. Mukundan, M. Konarova, L. Atanda, Q. Ma, J. Beltramini, Catal. Sci. Technol. 5 (2015) 4422–4432.

[28] N. Krishnankutty, M.A. Vannice, J. Catal. 155 (1995) 312–326.

[29] A. W. Scaroni, R.G. Jenkins, P.L. Walker, Appl. Catal. 14 (1985) 173–183.

[30] V.H.J. de Beer, F.J. Derbyshire, C.K. Groot, R. Prins, A.W. Scaroni, J.M. Solar, Fuel 63 (1984) 1095–1100.

[31] Y. Peng, S. Chen, Green Energy Environ. 3 (2018) 335–351.

[32] Y. Duan, Y. Liu, Z. Chen, D. Liu, E. Yu, X. Zhang, H. Fu, J. Fu, J. Zhang, H. Du, Green Chem. 22 (2020) 44–53.

[33] P. Hu, L. Yu, A. Zuo, C. Guo, F. Yuan, J. Phys. Chem. C 113 (2009) 900–906.

[34] T. Lin, J. Wang, L. Guo, F. Fu, J. Phys. Chem. C 119 (2015) 13658–13664.

[35] J. Shao, Q. Qu, Z. Wan, T. Gao, Z. Zuo, H. Zheng, ACS Appl. Mater. Interfaces 7 (2015) 22927–22934.

[36] Y. Zhang, Y. Li, H. Li, F. Yin, Y. Zhao, Z. Bakenov, J. Nanoparticle Res. 18 (2016) 1–9.

[37] C. Han, D. Zhu, H. Wu, Y. Li, L. Cheng, K. Hu, J. Magn. Magn. Mater. 408 (2016) 213–216.

[38] Y. Yi, X. Jin, L. Wang, Q. Zhang, G. Xiong, C. Liang, Catal. Today 175 (2011) 460–466.

[39] Q. Wang, S. Dong, D. Zhang, C. Yu, J. Lu, D. Wang, J. Sun, J. Mater. Sci. 53 (2018) 1135–1147.

[40] W. Zhang, L. Li, W. Zhu, H. Yan, S. Qi, J. Mater. Sci. Mater. Electron. 28 (2017) 15488–15494.

[41] A.S. Krishna Kumar, S.J. Jiang, J.K. Warchoł, ACS Omega 2 (2017) 6187–6200.

[42] H. Lu, J. Wang, H. Hao, T. Wang, Nanomaterials 7 (2017).

[43] Q. Pan, F. Zheng, X. Ou, C. Yang, X. Xiong, Z. Tang, L. Zhao, M. Liu, ACS Sustain. Chem. Eng. 5 (2017) 4739–4745.

[44] D. Lu, H. Wang, Q. Shen, K.K. Kondamareddy, D. Neena, J. Phys. Chem. Solids 106 (2017) 76–81.

[45] F. Lu, C. Xu, F. Meng, T. Xia, R. Wang, J. Wang, Adv. Mater. Interfaces 4 (2017) 1–14.

[46] S. Su, C. Zhang, L. Yuwen, X. Liu, L. Wang, C. Fan, L. Wang, Nanoscale 8 (2016) 602–608.

[47] S. Su, H. Sun, F. Xu, L. Yuwen, L. Wang, Electroanalysis 25 (2013) 2523–2529.

[48] M. Yi, C. Zhang, Tribol. Int. 116 (2017) 285–294.

[49] H.B. Park, Y.K. Lee, Fuel 239 (2019) 1265–1273.

[50] C. Ovalles, E. Rogel, M.E. Moir, A. Brait, Appl. Catal. A Gen. 532 (2017) 57–64.

[51] K.-D. Kim, Y.-K. Lee, J. Catal. 380 (2019) 278–288.

[52] K.D. Kim, Y.K. Lee, J. Catal. 369 (2019) 111–121.

[53] M. Daage, R.R. Chianelli, J. Catal. 149 (1994) 414–427.

[54] J.P.R. Vissers, B. Scheffer, V.H.J. de Beer, J.A. Moulijn, R. Prins, J. Catal. 105 (1987) 277–284.

[55] S. Sharifvaghefi, B. Yang, Y. Zheng, Appl. Catal. A Gen. 566 (2018) 164–173.

[56] J. Li, X. Wang, X. Tang, M. Zhang, X. Zheng, C. Wang, Z. Tang, Fuel Process. Technol. 188 (2019) 137–145.

[57] Y. Deng, D. Qi, C. Deng, X. Zhang, D. Zhao, J. Am. Chem. Soc. 130 (2008) 28–29.

[58] K. Zhao, X. Wang, H. Pan, Q. Li, J. Yang, X. Li, Z. Zhang, Appl. Surf. Sci. 427 (2018) 1080–1089.

[59] Y. Chen, Y. Wang, J. Lu, C. Wu, Fuel 88 (2009) 1426–1434.

[60] T. Liu, J. Lu, X. Zhao, Y. Zhou, Q. Wei, C. Xu, Y. Zhang, S. Ding, T. Zhang, X. Tao, L. Ju, Q. Shi, Energy and Fuels 29 (2015) 2089–2096.

[61] M.J. Ledoux, S. Hantzer, Catal. Today 7 (1990) 479–496.

[62] S. Dejonghe, R. Hubaut, J. Grimblot, J.P. Bonnelle, T. Des Courieres, D. Faure, Catal. Today 7 (1990) 569–585.

[63] T. Takahashi, H. Higashi, T. Kai, Catal. Today 104 (2005) 76–85.

[64] A.K. Rathi, M.B. Gawande, J. Pechousek, J. Tucek, C. Aparicio, M. Petr, O. Tomanec, R. Krikavova, Z. Travnicek, R.S. Varma, R. Zboril, Green Chem. 18 (2016) 2363–2373.

[65] M. Mahmoudi, N. Bertrand, H. Zope, O.C. Farokhzad, Nano Today 11 (2016)

817–832.

[66] S. Shylesh, V. Schünemann, W.R. Thiel, Angew. Chemie - Int. Ed. 49 (2010) 3428–3459.

[67] P.A. Montano, A.S. Bommannavar, J. Mol. Catal. 20 (1983) 393–403.

[68] T. Yang, C. Liu, W. Deng, C. Li, L. Gan, Q. Niu, Ind. Eng. Chem. Res. 58 (2019) 19072–19081.

[69] M.C. Biesinger, B.P. Payne, A.P. Grosvenor, L.W.M. Lau, A.R. Gerson, R.S.C. Smart, Appl. Surf. Sci. 257 (2011) 2717–2730.

[70] X. Lin, X. Wang, Q. Zhou, C. Wen, S. Su, J. Xiang, P. Cheng, X. Hu, Y. Li, X. Wang, X. Gao, R. Nözel, G. Zhou, Z. Zhang, J. Liu, ACS Sustain. Chem. Eng. 7 (2019) 1673–1682.

Prof Yang Liangrong graduated from the Department of Chemical Engineering of Tsinghua University in 2005, obtained a doctorate from the Institute of Process Engineering, Chinese Academy of Sciences in 2010, and she went to Massachusetts Institute of Technology (MIT) in USA as a postdoctoral visiting scholar in 2014, and obtained the the Li Foundation, Inc. funding. In 2010, she was a researcher at the Key Laboratory of Green Process Institute of Institute of Process Engineering, Chinese Academy of Sciences.

There are no conflicts to declare.